water

MDPI

Article

Sedimentary Processes and Instability on the Mississippi River Delta Front near the Shipwreck of the SS Virginia

Nathan Figueredo [1,*], Samuel J. Bentley [1], Jason D. Chaytor [2], Kehui Xu [3], Navid Jafari [4], Ioannis Y. Georgiou [5], Melanie Damour [6], Jeffrey Duxbury [1], Jeffrey Obelcz [7] and Jillian Maloney [8]

1 Department of Geology and Geophysics, Louisiana State University, Baton Rouge, LA 70803, USA; sjb@lsu.edu (S.J.B.); jeffrey.e.duxbury@gmail.com (J.D.)
2 United States Geological Survey, Lawrenceville, NJ 08648, USA; jchaytor@usgs.gov
3 Department of Oceanography and Coastal Sciences, Louisiana State University, Baton Rouge, LA 70803, USA; kxu@lsu.edu
4 Department of Civil and Environmental Engineering, Louisiana State University, Baton Rouge, LA 70803, USA; njafari@lsu.edu
5 The Water Institute, Baton Rouge, LA 70802, USA; igeorgiou@thewaterinstitute.org
6 Bureau of Ocean Energy Management, Sterling, VA 20166, USA; melanie.damour@boem.gov
7 Naval Research Lab, Washington, DC 20375, USA; jeffrey.obelcz@nrlssc.navy.mil
8 Department of Earth and Environmental Sciences, San Diego State University, San Diego, CA 92182, USA; jmaloney@sdsu.edu
* Correspondence: nfigue2@lsu.edu

Abstract: Sediment cores were collected from a mudflow lobe (80 m water depth) offshore of the Mississippi River's Southwest Pass in 2017 to better understand the sedimentology near the lobe entraining the SS Virginia shipwreck (sunk by a German U-boat in 1942) and surrounding Mississippi River delta front. Core analyses included ^{210}Pb/^{137}Cs geochronology, granulometry, and X-radiography. Sediment accumulation rates (SAR) calculated from excess ^{210}Pb activity in multicores are 0.22–0.29 cm/y at seabed depths less than 20 cm and 0.29–0.51 cm/y at depths greater than 20 cm. Accumulation rates for ^{137}Cs have been ~0.15 to ~0.37 cm/y since 1954 and 1963, respectively. Sediment accumulation rates from ^{210}Pb, ^{137}Cs geochronology and indicators of relative sedimentation and bioturbation from X-radiographs suggest that rates of sediment accumulation near the Virginia have declined since the mid-20th century. This may be explained by the multi-decade downslope mass transport of the mudflow lobe in which the shipwreck is embedded and decreases in sediment supply delivered offshore from the Mississippi river. Mass transport calculations of the Virginia lobe derived from core properties and published lobe advection rates suggest downslope mass transport is far higher than sediment resupply from the Mississippi river, consistent with recent studies of delta retreat.

Keywords: Mississippi river delta; sediment deposition; fine-grained sediment transport; sedimentary fabric; sediment gravity flow; slope stability

Citation: Figueredo, N.; Bentley, S.J.; Chaytor, J.D.; Xu, K.; Jafari, N.; Georgiou, I.Y.; Damour, M.; Duxbury, J.; Obelcz, J.; Maloney, J. Sedimentary Processes and Instability on the Mississippi River Delta Front near the Shipwreck of the SS Virginia. *Water* **2024**, *16*, 421. https://doi.org/10.3390/w16030421

Academic Editors: Yijun Xu, Giuseppe Oliveto and Heqin Cheng

Received: 20 December 2023
Revised: 17 January 2024
Accepted: 23 January 2024
Published: 27 January 2024

1. Introduction

1.1. Background

The Mississippi river delta front (MRDF) is an apron of sediment extending from a water depth of approximately 5 m to 200 m offshore of the southernmost distributaries of the Birdsfoot delta of the Mississippi River. The MRDF is sculpted by mass wasting processes that produce its distinctly irregular seafloor morphology of collapse features, gullies, and lobes [1,2]. Recent research has shown that large sections of MRDF seabed have begun to retreat in the last decades, after centuries of progradation [2,3]. Gagliano et al. identified subaerial retreat commencing as early as 1890 [4]. The cause of retreat [2,3], whether by erosion, mass-transport of sediment further downslope, anthropogenic modifications [5],

other processes, or a combination thereof, remains unknown. As part of a larger, multi-institutional study of the MRDF funded by the Bureau of Ocean Energy Management (BOEM), this study employed geological and geochronological analyses of sediment cores to elucidate sedimentary processes active in one mudflow lobe of the MRDF that is the resting place of the WWII shipwreck SS Virginia [6]. The SS Virginia is a bulk oil tanker that sank on 12 May 1942, after being hit by three torpedoes from a German U-boat and is a war grave. It was discovered in 2001 during an oil and gas survey. The shipwreck is intact; its bow points to the northwest, and it lists to its port side in 80 m of water embedded within a mudflow lobe produced by mass transport off Southwest Pass [6].

1.2. Study Area

This research primarily focused on the Virginia's location to the southeast of the Southwest Pass outlet (Figures 1 and 2) on the MRDF. The shipwreck is embedded within a mudflow lobe with a 2 m deep seafloor depression formed around the bow (Figure 2). The depression was present in 2017 but 2023 USGS bathymetry survey data that are being processed for release as of late 2023 (Jason Chaytor, personal communication) suggest that it may be gone. The location of the shipwreck has been tracked in historical bathymetric surveys by Chaytor et al., documenting the shipwreck's movement as follows [6]. The shipwreck was originally discovered during a 2001 high-resolution geophysical survey for oil-and-gas-related operations and confirmed as the Virginia in a 2004 remotely operated vehicle investigation. The shipwreck was later imaged ~365 m to the southeast during a post-hurricane Katrina pipeline survey in 2005–2006. A 2009 geophysical survey reported that the shipwreck was located ~54 m southwest of its 2006 position while surveys in 2016 and 2017 showed another ~6 m of southwestern movement. In total ~430 m of movement occurred over 2001–2004 and 2017 with a −4.5 m relief change and no changes in orientation. Over the 75 years before the 2017 survey, the Virginia has been displaced ~11 km downslope from where it reportedly sank. Regardless of the possible inaccuracies in the reported sinking location, that initial location serves as a starting point for estimated movement. The shipwreck appears to be conjoined strongly to the mudflow lobe and any recent movements of the shipwreck probably involved movement of the entire mudflow lobe [6]. South of the Virginia is the toe of the youngest mudflow lobe [5]. Approximate mudflow lobe boundaries are shown in Figure 2, encompassing an area approximately 2700 m by 2700 m in extent.

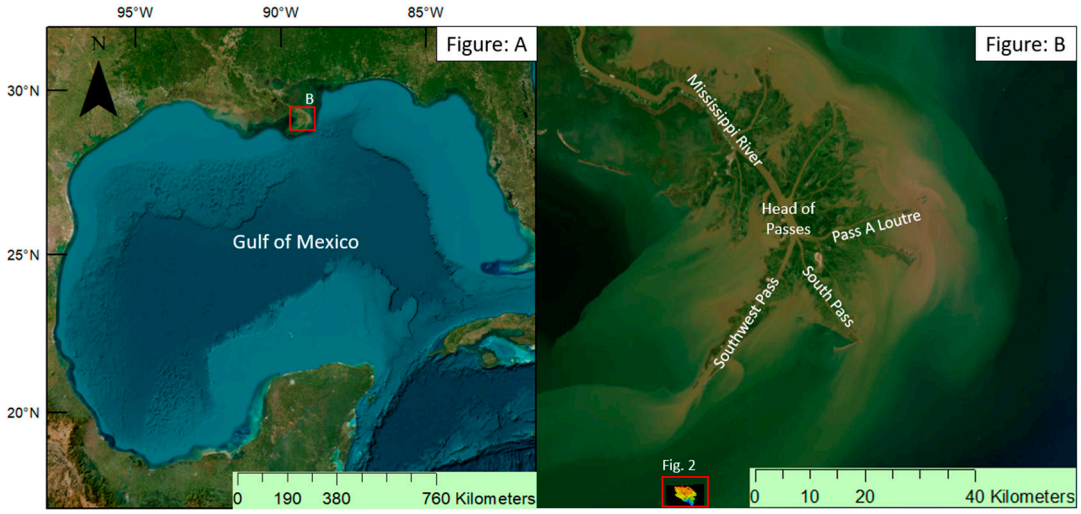

Figure 1. (**A**) Map of the Gulf of Mexico showing the location of the study area, B, within the gulf. (**B**) Map showing the Birdsfoot delta, within the Gulf of Mexico, highlighting the anatomy of the main distributary network.

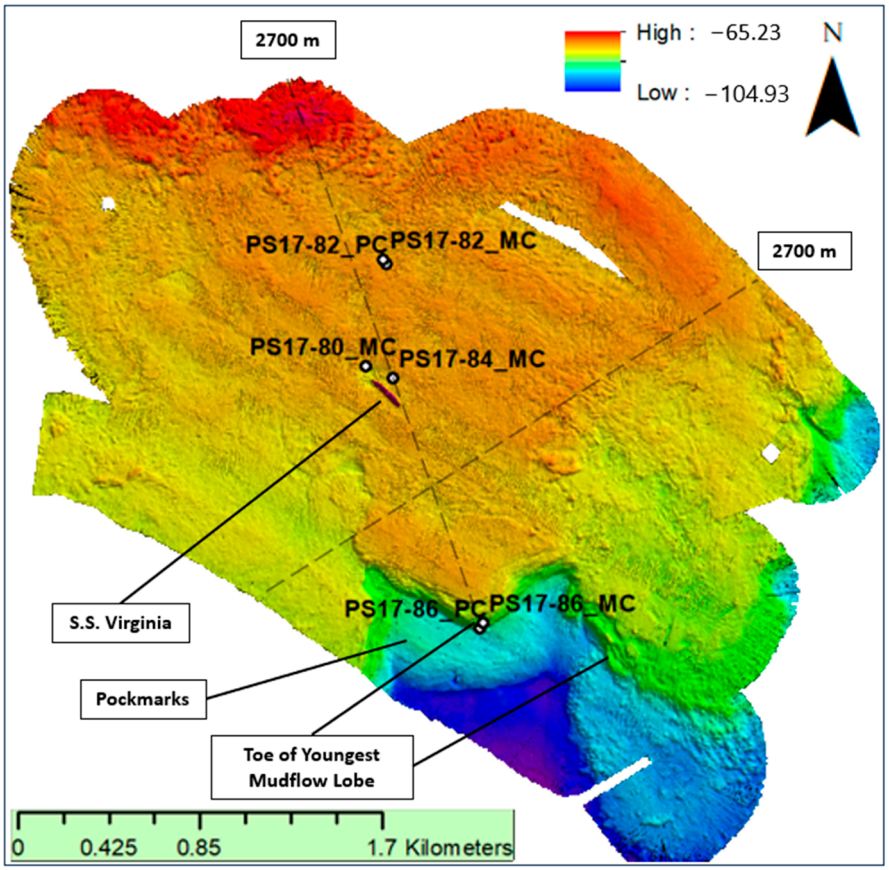

Figure 2. Depiction of the mudflow lobe, adapted from Chaytor et al., in which the 153 m long SS Virginia is locateds, with its bow pointed towards the northwest. A depression is in lighter colors near the bow. There are no drag or scar features on the lobe, indicating that the SS Virginia has been moving with the lobe rather than moving separately, across the lobe. Reprinted/adapted with permission from [6,7].

1.3. Hurricane Influence

Hurricanes increase sediment entrainment from the seabed at the onset of larger waves and higher currents offshore of the Mississippi River Delta [6]. Long-period waves associated with hurricanes can cause cyclic loading of the seabed that induces bottom shear stresses [1] resulting in sediment motion, including mass transport phenomena.

An example of the destructive capabilities of hurricane-induced mudflows is the Taylor Energy production platform (MC20A) that was destroyed by a hurricane-induced mudflow during hurricane Ivan (2004), resulting in substantial oil and gas release into the northern Gulf of Mexico as well as the dissolution of the Taylor Energy Company, costing at least USD 1 billion [8]. Guidroz conducted a risk assessment of hurricane-wave induced mudflows on the MRDF and identified the following criteria as necessary for producing waves strong enough to produce the largest mudflows: category 3 hurricane or larger, with slow transit across the MRDF region [9]. Hurricanes meeting these criteria since the onset of offshore oil and gas exploration in the 1950s and 1960s include Camille (1969), Ivan (2004), and Katrina (2005), each of which shifted large portions of MRDF mudflow lobes (including the Virginia lobe from at least hurricanes Ivan and Katrina), and damaged seabed infrastructure [9,10]. The continued tracking of the Virginia and other nearby shipwrecks are important aspects of multi-component hazard vulnerability risk assessments, because of the cultural and historical importance of these sites (the National Historic Preservation Act of 1966 (54 USC § 306108)), and their utility as tracers for seabed motion.

1.4. Sediment Properties and the SS Virginia

Subaqueous sedimentary deposits of the Mississippi river delta are controlled by seasonally and annually varying external inputs, such as river sediment delivery or storms, and quasi steady-state internal processes, such as sediment consolidation or biogenic gas production/release [2,6]. This study area is affected by multiple sediment dispersal processes, including hypopycnal river plumes [11–13], storm wave/current-induced resuspension [14], sediment slides driven by gravity acting on a slope [2], and possibly wave/current-enhanced sediment gravity flows [15], although this type of flow has not yet been observed directly on the MRDF. The subaqueous delta is also now showing the effects of both recent and long-term declines in sediment supply [3,16]. This change is manifested as the first observed transgression of the subaqueous delta, indicated by the landward migration of 10 m isobaths near the three main historical river outlets, and upstream migration of substantial river discharge to new and expanding outlets upstream of the three major historic outlets (Figure 1) [16]. Interaction of these processes control the morphology and morphodynamics of the study area. In addition to historical and recent changes in sediment supply from the river [16], the downslope advection of the Virginia lobe should impact sediment accumulation rates on the lobe from the mid-20th century onwards, by changing the local sediment supply and depositional setting of the Virginia sediment lobe, causing sediment accumulation rates (SARs) to decline over time due to both changing flux from the river and changing depositional setting (due to lobe motion).

The rationale for this research is twofold: first, to better understand sediment-specific site formation processes near the shipwreck for the purposes of marine archaeological research, and, second, to inform our understanding of the dynamics of sediment motion in the study area, forced by both hydrodynamic and gravity-driven phenomena. This is possible in part because the shipwreck's location can be used as a tracer of seabed movement [6].

2. Materials and Methods

2.1. Field Work and Core Processing

In June 2017, a U.S. Geological Survey (USGS) cruise on the R/V Point Sur conducted a high-resolution geophysical survey across the MRDF [6,7]. A second cruise in 2017 led by Louisiana State University (LSU) collected piston cores and multicores (Table 1) from specific depositional settings mapped by the USGS. Samples were collected using a Benthos piston corer (core diameter of 7.5 cm), capable of collecting cores of up to 8 m depth in seabed, and an Ocean Instruments MC-800 multicorer (core diameter of 10 cm), that collects sediment with limited disturbance up to 50 cm depth. Observations during core collection of all piston cores revealed evidence of gas expansion when processing cores on deck. Piston cores PS17-82-PC and PS17-86-PC were selected to provide data on opposing sides of the shipwreck site. Multicores PS17-80-MC and PS17-84-MC were selected due to their central positioning on the lobe as well as being ~80 m and ~50 m from the Virginia. PS17-86-MC was added for comparison with its piston core PS17-86-PC in order to account for sediment non-recovery from the top 50 cm of the corresponding piston core. The positioning of the selected cores can be seen in Figure 2. Rectangular slabs were extracted from multicore tubes onboard the ship for subsequent imaging, and one multicore tube per deployment was extruded and sliced at 2 cm intervals for radiochemical and granulometric measurements, with subsamples refrigerated in sealed plastic bags until analysis.

Cores were returned to LSU and kept in refrigeration pending analysis. Grain size distributions, sediment fabric, radionuclide distributions, and gamma density, were measured and interpreted in conjunction with the geophysical survey data from the 2017 USGS surveys to elucidate dominant sedimentary processes and their spatial and temporal patterns. Gamma density for piston cores was measured in July 2017 using a Geotek Multi Sensor Core Logger (MSCL) (manufactured by Geotek in St. Cloud, MN, USA).

Table 1. Summary of collected piston and multicores.

Station	Distance from SW Pass (km)	Distance from SS Virginia (m)	Depth from Sea Level (m)	Penetration Depth (cm)
PS17-80-MC	18.99	150	84.7	18
PS17-82-MC	18.49	612	83.7	40
PS17-84-MC	19.03	69	84.3	28
PS17-86-MC	20.17	1174	88.8	34
PS17-82-PC	18.5	595	83.8	862
PS17-86-PC	20.14	1192	89	564

2.2. Sedimentological Analyses

Granulometric analyses were conducted on samples extracted at 2 cm intervals from the cores using a Beckman-Coulter LS13-320 laser (manufactured by Danaher in Washington, DC, USA). Diffraction instrument following the methods of Restreppo et al. [17]. Core slabs for X-radiography sedimentary fabric analysis were imaged using a Samsung Model SP501 (manufactured by Samsung in Suwon-si, South Korea). X-ray digital detector panel illuminated by a Min Xray HF-80 X-ray generator (manufactured by Min-Xray in Nothrbrook, IL, USA) and evaluated for sedimentary fabric and macrostructures using the image processing program Image-J 1.54h (developed by Wayn Rasband). Split piston cores were imaged using an aluminum compensation plate machined to a parabolic profile to even exposure of the half-round slabs, refining an approach developed by Baker and Friedman for film-based radiography [18].

2.3. Radionuclide Analysis

Sediment was subsampled for granulometric and radiochemical analyses from multicores at 2 cm intervals, and every 12 cm for working halves of split piston cores. Intervals were selected to provide adequate resolution for dating without being too costly in detector time. The primary radionuclides of interest are excess ^{210}Pb (natural ^{238}U series, $t_{1/2}$ = 22.2 years) and ^{137}Cs (anthropogenic fallout, $t_{1/2}$ = 30.1 years). ^{210}Pb and ^{137}Cs are absorbed, like many other particle-reactive elements, by settling particles and thus trace the pathway of depositing sediments [19]. Data are reported in decays per minute per gram dry sediment (dpm/g), where 1 dpm = 60 Bq.

Samples were dried and then ground using a mortar and pestle and sealed into petri dishes. Samples rested in sealed dishes for 14 days before ^{210}Pb data were collected, which allowed ingrowth of ^{210}Pb parent radionuclide ^{222}Rn and to determine supported activities. All samples were analyzed on Canberra BEGe 3825 detectors calibrated for energy and efficiency using standard reference materials with samples from a single core being restricted to one detector. ^{137}Cs was measured using the 661 keV peak for that radioisotope, with a detection limit of ~0.1 dpm/g. Sample self-absorption for ^{210}Pb gamma emissions was determined using the transmission method [20]. Activities associated with the 295 and 352 keV peaks of ^{214}Pb and the 609 keV peak of ^{214}Bi were averaged to determine the amount of supported ^{210}Pb. Supported ^{210}Pb activity is subtracted from total ^{210}Pb activity to determine excess ^{210}Pb activity.

For ^{137}Cs geochronology, we assume, based on Nittrouer et al., that (1) ^{137}Cs was introduced into the environment in 1954 and was rapidly transferred to depositing sediments; (2) ^{137}Cs activities reached maximum values in the atmosphere in 1963; and (3) upon deposition, ^{137}Cs-laden sediments are rapidly mixed to the base of the bioturbated zone, described as sediment deposits being disturbed by living organisms [21]. The accumulation rate based on ^{137}Cs can then be calculated from Equation (1):

$$A = ((z_{max}) - z_b)/(2017 - (1963 \text{ or } 1954)) \quad (1)$$

where A is the accumulation rate (cm/y), z_{max} is the depth of maximum ^{137}Cs (cm) for either 1954 (first appearance of ^{137}Cs) or 1963 (peak activity of ^{137}Cs), z_b is the depth of bioturbation (cm), and 2017 is the year cores were collected [21].

Dominant processes that can influence the distribution of excess ^{210}Pb and other radionuclides in the shallow seabed include sedimentation (termed "advection" by Berner [22]), radioactive decay, bioturbation, and erosion. The intent of this analysis is to use ^{210}Pb data from the cores to model SAR and D_b, which are calculated using excess ^{210}Pb. An overall review of radiochemical and sedimentary fabric data was used to determine the most appropriate approach to model the observed range of conditions. In settings where erosion depths are much less than thicknesses of sediment deposited, erosion is often ignored [23]. For ^{210}Pb geochronology, steady-state conditions are assumed, and rates of bioturbation and sediment accumulation can be evaluated from Equations (2)–(4). For sediments containing excess ^{210}Pb that are below the depth of bioturbation, long-term sedimentation rates (SAR) can be calculated from Equation (2) (adapted from Aller and from Nittrouer and Sternberg [23,24]). For conditions where bioturbation (represented as biodiffusion) and sediment accumulation are both important, Equation (3) is used [23,24]. For conditions where bioturbation and sediment accumulation are equally important in transporting sediments within the seabed, Equation (4) is used [23,24].

$$A_z = A_0\, e^{(-\lambda\, z/S)} \tag{2}$$

$$A_z = A_0 \exp[(-z/\sqrt{(D_b/\lambda)}] \tag{3}$$

$$A_z = A_0 \exp[z \cdot (S - \sqrt{(S^2 - 4D_b\lambda)})/2D_b)] \tag{4}$$

where A_z is activity at depth z (dpm/g), A_0 is activity extrapolated to the sediment surface (dpm/g), λ is the decay constant of radionuclide of interest (y^{-1}), S is the sediment accumulation rate (cm/y), and D_b is the biodiffusion coefficient (cm^2/y). Values for S, D_b, and A_0 were calculated using nonlinear least squares regressions after Muhammad et al. [25]. In addition, the age of the ^{210}Pb-laden deposit can be calculated by dividing the mean depth of the layer by the deposition rates obtained by Equation (4) [2].

Patterns of excess ^{210}Pb activity in sediment cores that suggest unsteady ^{210}Pb delivery (including multiple breaks in log–linear slopes, and undulatory profiles in log–linear plots) can indicate specific depositional processes. For example, fine sediment river plumes can deplete ^{210}Pb activity in marine waters, yielding sediment beds of fine grain size and low ^{210}Pb activity [2,26]. Sediment resuspension and deposition through storm activity and sediment gravity flows produces beds that fine upward and may contain stair-step patterns in ^{210}Pb activity. Horizontal "step treads" may represent erosional bed contacts and uniform riser activity may correspond with deposited beds wherein sediment has been homogenized, producing vertically uniform ^{210}Pb activities. Additionally, variations in ^{210}Pb activity can be associated with grain size distribution with sands having lower ^{210}Pb activity than muds [2].

3. Results

3.1. Granulometry

Grain size volume frequency plots are shown for multicores in Figures 3–5 and piston cores in Figures 6 and 7. Overall, silt is the dominant grain size fraction, comprising ~70–90% of the samples. Granulometric data show a modal distribution in the very fine silt range (8–10 μm), indicated by warm colors in those plots. The clay sized material fraction content comprises 10–20% and sand content is 0–5%.

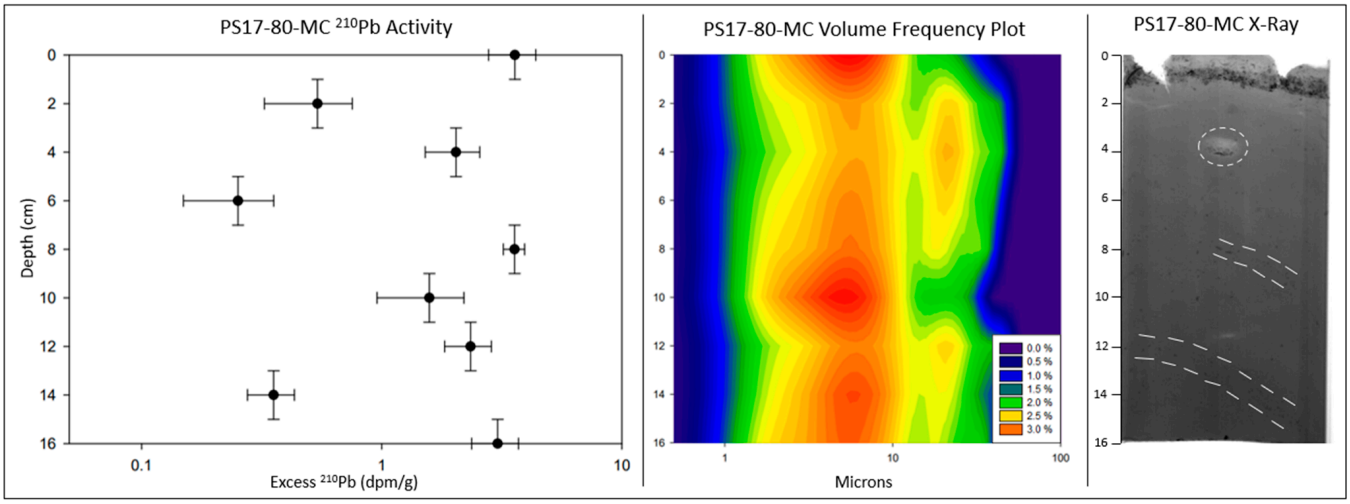

Figure 3. Excess ^{210}Pb, grain-size frequency plot, and X-radiographic imaging of multicore PS17-80-MC, immediately north of SS Virginia. X-radiographic images display higher density sediment as darker gray shades, lower density sediment as lighter gray, and voids as white. The white dashed lines in the X-radiographic image highlight burrows outlined by iron flakes.

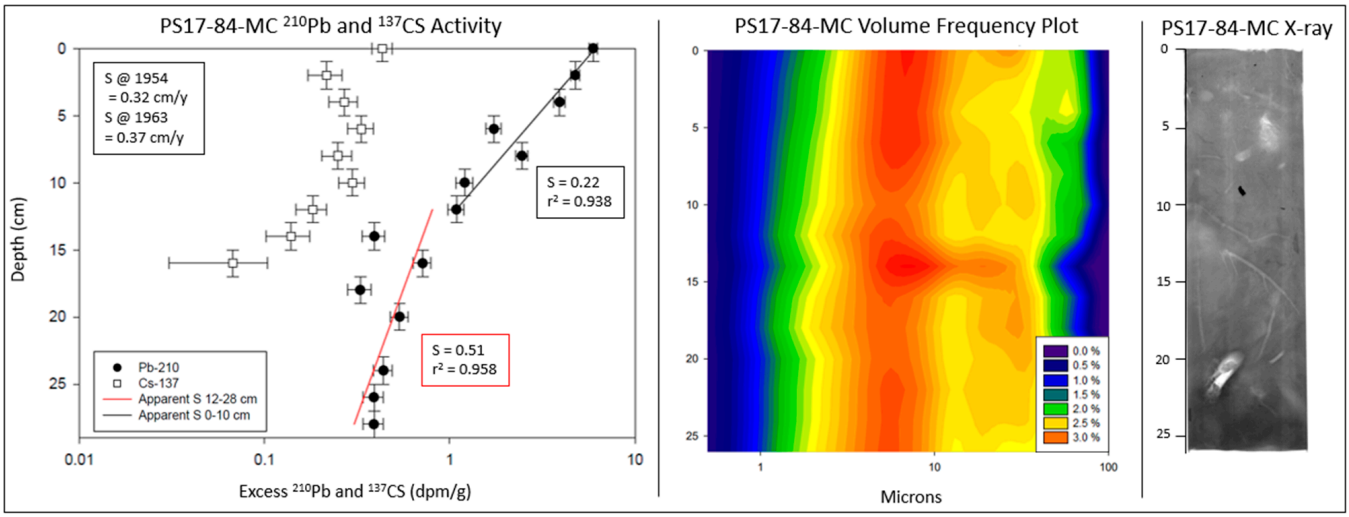

Figure 4. Excess ^{210}Pb and ^{137}Cs profiles, grain-size frequency plot, and X-radiographic imaging of multicore PS17-84-MC, east of SS Virginia. X-radiographic images display higher density sediment as darker gray shades, lower density sediment as lighter gray, and voids as white.

For the multicores, PS17-80-MC (Figure 3) was collected ~80 m from the shipwreck (Figure 2). Sediment is fine-grained with generally homogenous grain size distribution, except for slight coarsening at 2–6 cm and 12–14 cm depth, associated with iron oxide (rust) grains that are visible in the X-radiograph. PS17-84-MC (Figure 4) is generally homogenous excepting a slightly coarser zone near 14 cm depth. PS17-86-MC (Figure 5) coarsens slightly in modal grain size from bottom to top, from near ~7 µm at 25 cm depth to ~10 µm at the sediment–water interface.

For the piston cores, the cores shown in Figures 6 and 7 penetrated 5–8 m into the seabed and display much greater granulometric variability over these larger depth scales than do the short multicores. Both piston cores display generally bimodal variations downcore peaking at 84 µm in PS17-82-PC and 63 µm in PS17-86-PC (Figures 6 and 7).

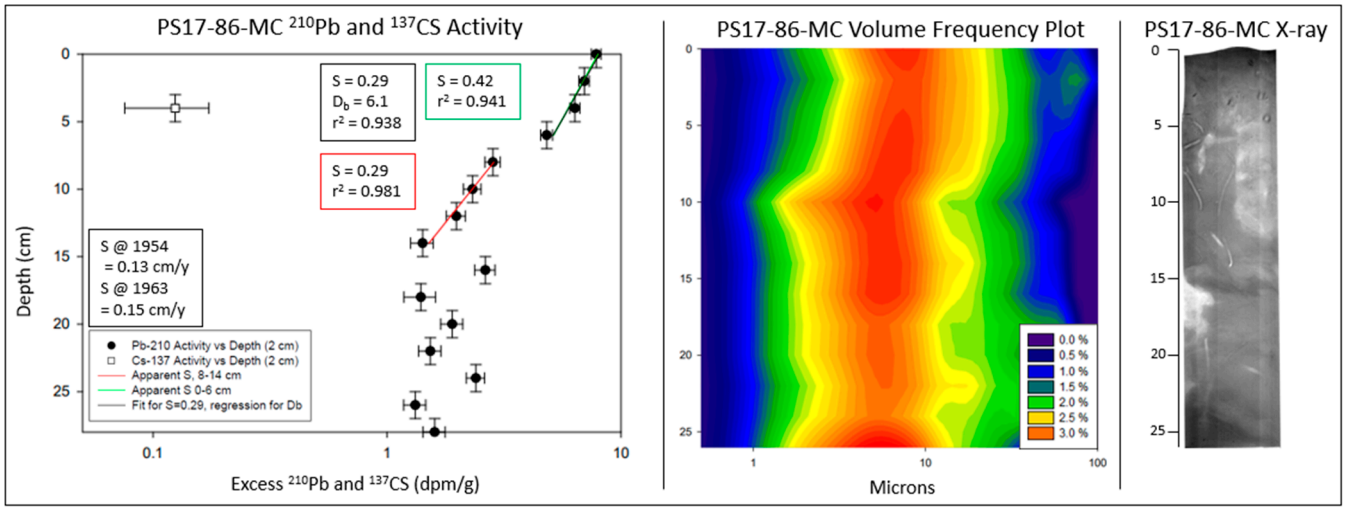

Figure 5. Excess ^{210}Pb and ^{137}Cs profiles, grain-size frequency plot, and X-radiographic imaging of multicore PS17-86-MC, at the toe of the mud lobe south of SS Virginia. X-radiographic images display higher density sediment as darker gray shades, lower density sediment as lighter gray, and voids as white.

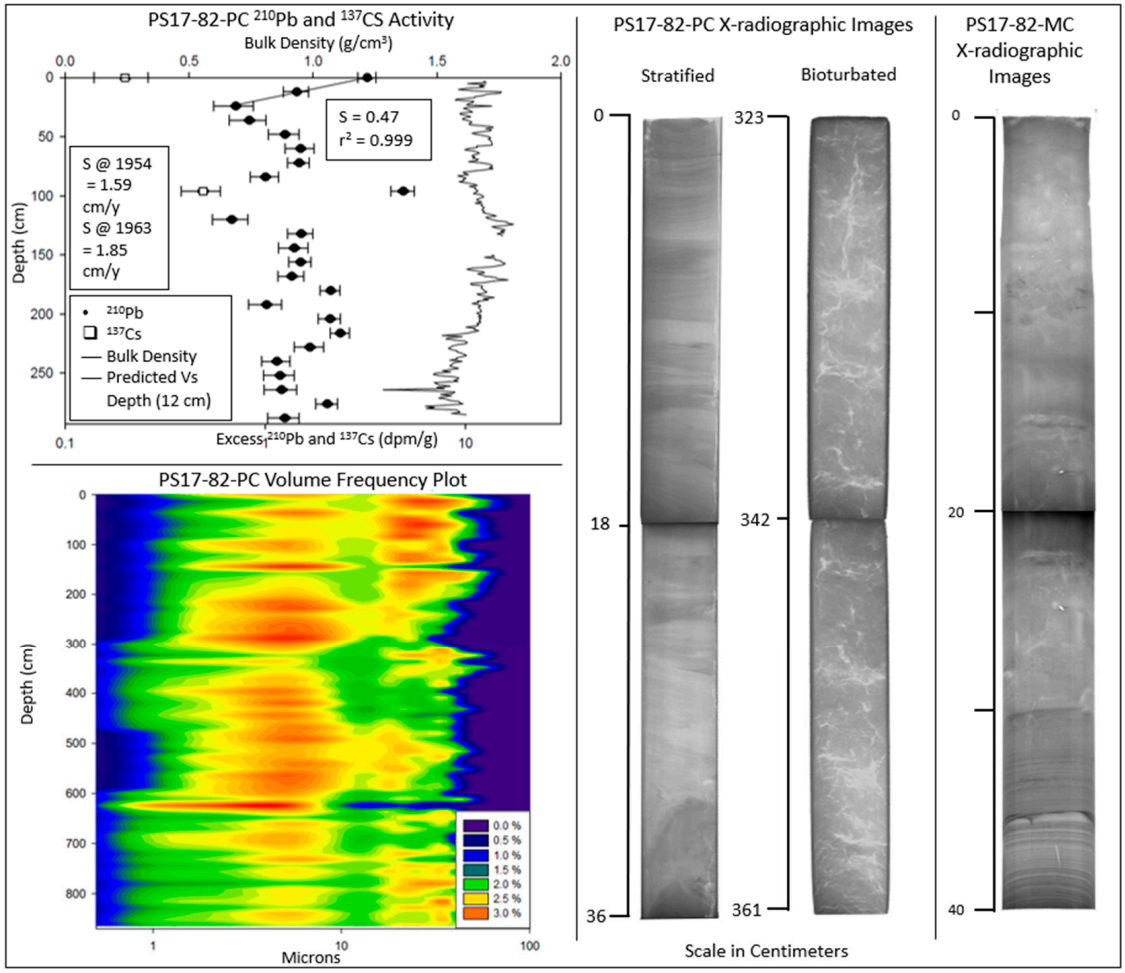

Figure 6. Excess ^{210}Pb and ^{137}Cs profiles, grain-size frequency plot, and X-radiographic imaging of piston and multicore PS17-82-PC, MC, at the northmost portion of the mud lobe. X-radiographic images display higher density sediment as darker gray shades, lower density sediment as lighter gray, and voids as white.

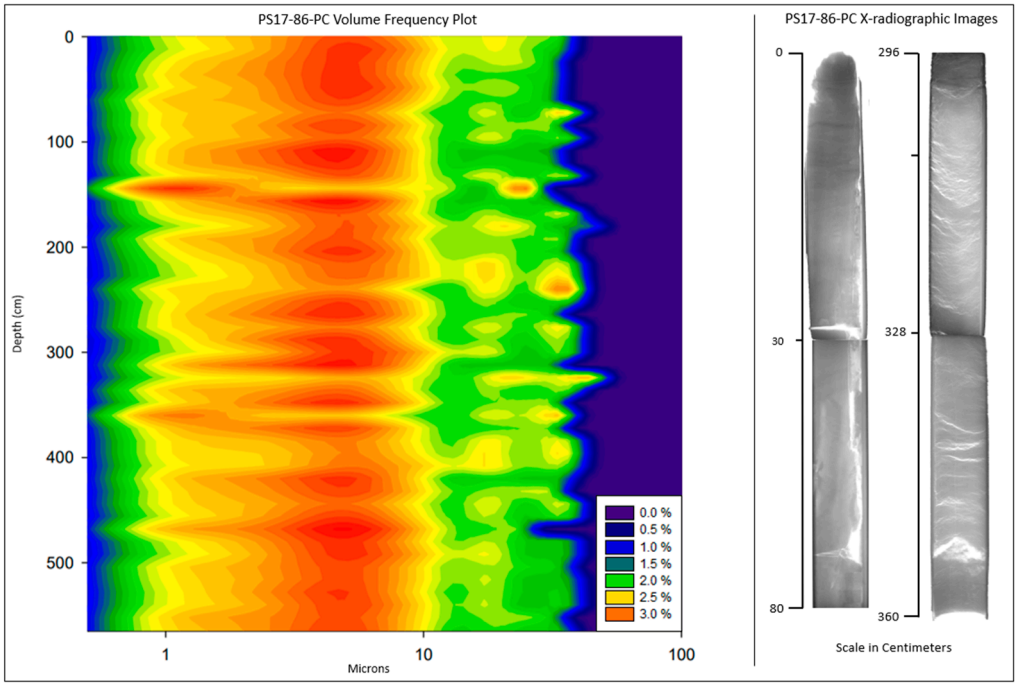

Figure 7. Grain-size frequency plot and X-radiographic imaging of piston core PS17-86-PC, at the toe of the mud lobe. X-radiographic images display higher density sediment as darker gray shades, lower density sediment as lighter gray, and voids as white.

3.2. X-Radiography

X-radiographs are scaled to display higher density sediment as darker gray shades, lower density sediment as lighter gray, and voids as white. This allows for the visual identification of differing sedimentary fabrics and structures. Overall, X-radiographic images reveal the following four classes of sedimentary fabric and structures: biogenic mottling and biogenic sedimentary structures; stratified sediment layers that are likely the result of sediment deposition; inclined stratification; and light-gray-to-white regions that are likely voids produced by biogenic gas expansion during core retrieval.

For the multicores, PS17-80-MC (Figure 3) images show a stratified surface layer containing a layer of low-density sediments on top of iron oxide grains in the 0–2 cm depth interval, above mostly homogeneous sediment with a large, open burrow near 4 cm depth, and inclined burrows highlighted by iron oxide grains at 8–16 cm depth. PS17-82-MC (Figure 6) images show biogenic mottling and faintly stratified sediments in the upper ~30 cm, underlain by less bioturbated and more stratified sediment at 30–40 cm depth. Laminations and texture visible in X-radiographs in this interval appear similar to those at the 0–15 cm depth interval of PS17-82-PC. PS17-84-MC (Figure 4) images show bioturbation with large, open, and partially filled outward facing and lengthwise burrows. Rust flakes (also identified during core subsampling for granulometry and radiochemistry) are also scattered throughout the core. PS17-86-MC (Figure 5) primarily shows bioturbation with faint physical stratigraphy near the bottom and lengthwise burrows. The faintly stratified lower section of the core is interpreted as evidence for rapid muddy deposition.

For the piston cores, core PS17-82-PC was collected within ~100 m of multicore PS17-82-MC (Figures 2 and 6) and lacks the surficial zone of bioturbated sediments found in PS17-82-MC. This suggests that PS17-82-PC did not recover the uppermost ~30 cm or more of the seabed. Deeper sediment displays faint centimeter-scale mottling and decimeter-scale variations in apparent density that may be remnant (unbioturbated) bedding. Below ~200 cm depth, arcuate sub horizontal voids likely created by gas expansion, observed during on-ship core processing, are evident to the base of the core at 825 cm. PS17-86-PC (Figure 7) shows faintly stratified sediments in the top 15 cm of the core. From 15 cm to the base of the core, centimeter-scale mottling and faintly bedded light-to-dark-gray regions

are apparent. Below ~200 cm depth, arcuate sub horizontal voids created by gas expansion occur to the base of the core at 564 cm depth.

3.3. Radionuclide Analysis

For the multicores, PS17-80-MC activity shows heterogenous vertical ^{210}Pb (0–16 cm) distribution and no obvious trends with depth (Figure 3), and ^{137}Cs is not detectable. No estimates of bioturbation or sediment accumulation are possible with these data using Equations (2)–(4) due to short core length and lack of a useful gradient or trend in the ^{210}Pb profile (required for application of Equations (2)–(4)).

PS17-84-MC activity has two separate gradients of ^{210}Pb activity versus depth that can be identified (Figure 4). Over 0–12 cm depth, an irregular log–linear gradient declines from the sediment–water interface. Over 12–25 cm, a variable and more vertical log–linear gradient is evident. If a regression for sedimentation and decay is applied (Equation (2)), accumulation rates are 0.22 cm/y over 0–12 cm and 0.51 cm/y deeper in the core. However, given the mottling evident in the X-radiograph for this core, it is likely that bioturbation also influences the ^{210}Pb gradient over 0–12 cm. If so, then the actual ^{210}Pb sediment accumulation rate is likely to be lower to account for the mixing effects of bioturbation. A well-defined ^{137}Cs profile is evident, with ^{137}Cs first occurring at 16 cm depth and a subsurface maximum of 8 cm depth. From Equation (1), accumulation from ^{137}Cs is 0.32 cm/y since 1954, assuming a depth of rapid bioturbation of ~6 cm (estimated below). When rates are calculated from the peak value of ^{137}Cs that is assumed to represent ca. 1963, the ^{137}Cs sediment accumulation rate since 1963 is 0.37 cm/y.

PS17-86-MC shows three distinct zones of excess ^{210}Pb, with ^{137}Cs detectable only in one sample at 4 cm depth (Figure 5). The ^{210}Pb activity over 0–6 cm depth shows a steep sub-vertical log–linear decline. At 8–14 cm, a regular but less vertical decline is evident, below which the profile is vertical and irregular. The uppermost two zones define a profile consistent with marine–sedimentary ^{210}Pb analyses [25], influenced mostly by bioturbation in the upper zone, and mostly by sediment accumulation in the lower zone, with radioactive decay active throughout. For regression analysis, the middle zone of the ^{210}Pb profile yields a sediment accumulation rate of 0.29 cm/y for 8–14 cm (Equation (2)). Using this value for sediment accumulation in a regression of Equation (4) over the 0–6 cm zone yields $D_b \approx 6$ cm^2/y (Table 2). The irregular vertical basal profile of excess ^{210}Pb suggests rapid deposition or mixing in this interval. If the 0–6 cm were SAR only, the SAR only regression (Equation (2)) would be 0.42 cm/y. The presence of a single detection of ^{137}Cs at 4 cm is difficult to assess. Two possibilities include earliest introduction (1954) or peak value (1963). If it were the first introduction, then sediment rates based on ^{137}Cs since 1954 would be 0.13 cm/y or less, depending on effects of bioturbation. If it were the peak value, then sediment rates based on ^{137}Cs since 1963 would be 0.15 cm/y or less, depending on the effects of bioturbation.

Table 2. Summary of radionuclide regression analysis.

Station	^{210}Pb SAR (cm/y)	r_2	^{210}Pb Depth Range (cm)	^{210}Pb SAR (cm/y)	r_2	^{210}Pb Depth Range (cm)	D_b	r_2	D_b Depth Range (cm)	^{137}Cs SAR 1954 (cm/y)	^{137}Cs Depth Range (cm/y)	^{137}Cs SAR 1963 (cm/y)	^{137}Cs Depth Range (cm/y)
PS17-84-MC	0.22	0.938	0–12	0.51	0.958	12–25	N/A	N/A	N/A	0.32	0–16	0.37	0–8
PS17-86-MC	0.42	0.941	0–6	0.29	0.981	8–14	6.1	0.938	0–6	0.13	0–4	0.15	0–4
PS17-82-PC	0.47	0.999	0–24	N/A	N/A	N/A	N/A	N/A	N/A	1.59	0–96	1.85	0–96

For the piston cores, in PS17-82-PC excess ^{210}Pb is present over 0–200 cm, with a rapid decline with increasing depth over 0–24 cm, and a highly irregular but generally approximate vertical profile below 24 cm. At 0 and 96 cm, ^{137}Cs is present (and this may be present at other depths but below detection limits of ~0.1 dpm/g). Because this depth interval is unbioturbated, a regression using Equation (2) (sediment accumulation and decay) for ^{210}Pb is appropriate and yields an SAR of 0.47 cm/y for 0–24 cm. It is uncertain

whether the ^{137}Cs detected at 96 cm is closer to the first introduction or the peak value. If it were the first introduction, then sediment rates based on ^{137}Cs since 1954 would be 1.59 cm/y. If it were the peak value, then sediment rates based on ^{137}Cs since 1963 would be 1.85 cm/y. However, the two detections of ^{137}Cs over 96 cm provide few reference points for SAR estimation.

PS17-86-PC does not contain any excess ^{210}Pb or detectable ^{137}Cs, suggesting the uppermost tens of cm of sediment were either not recovered in the piston core, or were removed from the seabed by physical processes prior to coring.

3.4. Piston Core Density

Both piston cores show cm scale and m scale variations in density downcore, over density ranges of 0.1 g/cc for cm scale variations and 0.4 g/cc for m scale variations (Figure 8).

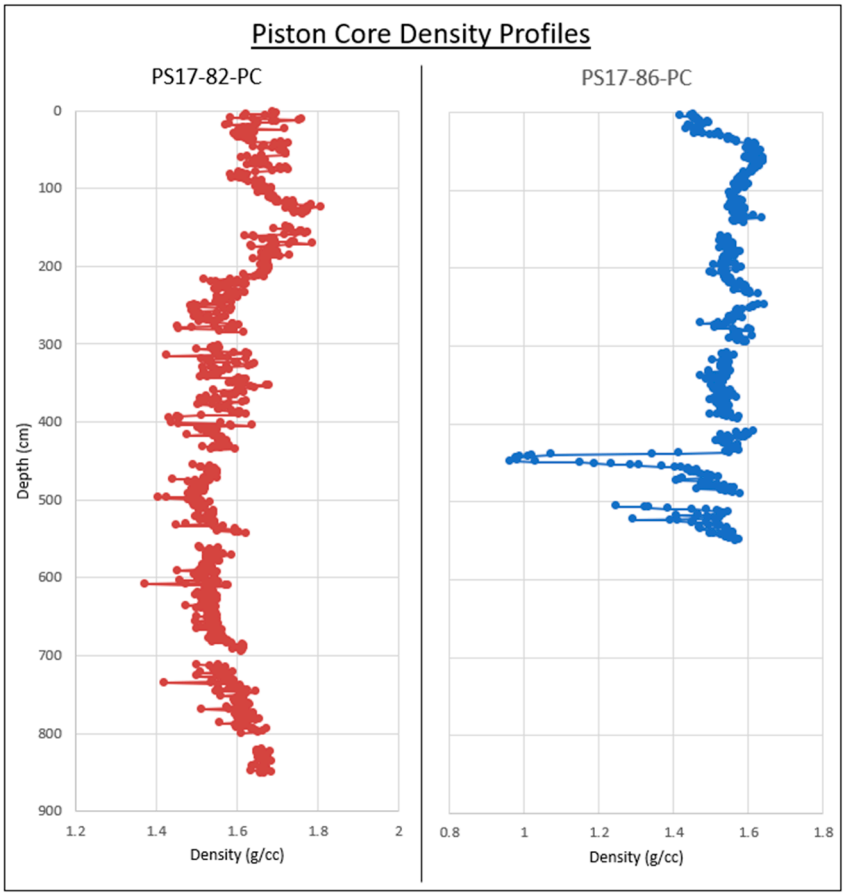

Figure 8. Density profiles of piston cores PS17-82 and PS17-86 at their respective depths. Artifacts in density measurements created by open voids were removed.

PS17-82-PC displays sawtooth variations of ~0.1–0.2 g/cc occurring at the centimeter scale over 4–24 cm and 40–81 cm intervals. A gradual downward increase occurs over 88–134 cm, below which density declines with variations downward from ~1.75 g/cc at 150 cm depth to ~1.6 g/cc at 250–400 cm depth. From 400 to ~675 cm depth, density varies around ~1.55 g/cc, then increases slowly to the base of the core, at ~1.65 g/cc.

PS17-86-PC's density increases sharply over 28–38 cm by ~0.3 g/cc. A slight density decrease of ~0.03 g/cc occurs at 41–79 cm, then varies in the range of 1.5–1.6 g/cc from 100 to 200 cm depth. Density then increases slightly to ~1.65 g/cc at 250 cm depth, then declines downward to ~1.55 g/cc over the 325–425 cm depth range.

4. Discussion

4.1. Rates and Distances of Lobe Motion

The movement of the Virginia and its associated sediment lobe constitute one of the few multi-year and unambiguous records of large-scale, gravity-driven mass transport on the MRDF. Its historical movement over a 75-year period—especially over the last two decades—highlights that both slow and rapid movement can occur [6]. Movement of the shipwreck is assumed to track that of the surrounding mudflow lobe because the two appear to be conjoined. If the reported 1942 sinking location is the approximate point the vessel came to rest on the seafloor, and excluding undocumented hurricane-induced motion, the shipwreck site would have moved at an average rate of 147 m/y. Relative to discrete block movements measured within MRDF mudflow gullies, this rate is nearly double the 85 m/y maximum 2016–2017 rate reported by Chaytor et al. at Southwest Pass, but close to the maximum 141 m displacement over a two-month period reported by Galloway et al. in a gully east of Southwest Pass [6,27]. From 2004 to 2017, the rate of motion was 30.7 m/y, becoming stationary during 2016–2017.

Guidroz synthesized and analyzed observations for the movement of large MRDF sediment lobes due to the cyclic loading of the MRDF seabed by major hurricane waves [9]. Guidroz's analysis suggests that the substantial increases in lobe movement rate during periods of intense hurricane activity (2004–2006 and 2007–2009) are likely caused directly by hurricane activity and suggests that instantaneous rates (that have not yet been measured) might be even more rapid than the time-averaged displacement rates of Chaytor et al. [6,9]. This motion over 75 years appears to have transferred the shipwreck and sediment lobe from a location near to the river outlet (with associated high SARs of 1.3–7.9 cm/y, as per the study of Maloney et al. and references therein) to a region farther from the river outlet, where present SARs appear to be generally lower (Table 2) [2].

4.2. Radioisotope Geochronology and Sedimentary Fabric

Results of core analysis near the Virginia exhibit some consistent trends among cores. Radionuclide data of multicores PS17-84-MC and PS17-86-MC show historically faster sediment accumulation overlain by slower recent sediment accumulation and pervasive near-surface bioturbation in the vicinity of the shipwreck. PS17-80-MC is a short core that is not suitable for ^{210}Pb geochronology and does not reach the sediment-depth ranges of historical rapid sedimentation in other cores. However, it does exhibit signs of bioturbation in shallow sediments in X-radiographic images, suggesting slow sedimentation overprinted by bioturbation within the short depth of the core (like surface sediments in other multicores). For PS17-84-MC and PS17-86-MC, the bioturbation terms incorporated into the radionuclide regression analysis (represented as biodiffusion coefficient D_b and the apparent mixing depth L_b) are consistent with X-radiographic imaging showing evidence of bioturbation, especially in the shallowest sediments. Each core contains two or more zones characterized by downward changes in ^{210}Pb gradients, which represent shifts from high SARs, likely near and before ca. 1953 (when ^{137}Cs first appears in marine sediments globally). The top sections of PS17-82-PC and PS17-82-MC show consistency with the other multicores, suggesting steady sedimentation overlain by bioturbation. For PS17-82-PC below~24 cm, no SAR can be determined using Equations (2)–(4); however, such irregular near-vertical profiles of excess ^{210}Pb have been associated with periods or events of rapid sediment deposition. Where evidence for steady sedimentation is present, SARs range between 0.42 and 0.51 cm/y. PS17-84-MC has the most complete ^{137}Cs profile. This allows for identification of first appearance at ~16 cm and peak activity at ~6 cm. Based on first appearance; the sedimentation rate based on ^{137}Cs profile are 0.32 cm/y. This is consistent with sedimentation rate calculations based on ^{210}Pb activity (Table 2, Figures 3–5).

Sedimentary fabric in X-radiographic images shows fabric similarities among multicores, supporting the ^{210}Pb regression analysis. Multicores PS17-80-MC and PS17-84-MC are extensively bioturbated through the shallowest 12 cm, consistent throughout all cores for which the sediment–water interface was likely recovered. PS17-82-MC and PS17-86-MC

show bioturbation near the surface as well as fully/partially stratified sections buried beneath. This is generally consistent with what is seen in the piston core sedimentary fabric and geochronology described for PS17-82-PC and PS17-86-PC. For instance, PS17-82-PC continues the stratification that is seen in the lower portion of its multicore counterpart. PS17-86-PC shows similar results; however, its stratification is much fainter and potentially partially bioturbated in the multicore.

PS17-80-MC is located within the depression at the bow of the shipwreck. This depression could be a current scour near the ship that hinders deposition and accumulation, potentially explaining its shallow penetration depth, short/irregular vertical ^{210}Pb profile and the lack of detectable ^{137}Cs. Collectively, this could be explained by the erosion and bypass of both historically ^{137}C-laden sediments as well as freshly deposited sediments with naturally elevated excess ^{210}Pb activities.

Downcore changes in apparent SAR and the vertical patterns of bioturbation (highest near the sediment surface) and stratification in core X-radiographs (generally more stratified towards the base of cores) together suggest that sediment delivery to the Virginia lobe may have declined over the last century. The presence of stratified sediment in multicores PS17-82 and PS17-86 below the 34 cm depth horizon suggests a recent relative increase in the degree of bioturbation in the sedimentary fabric. Bioturbating invertebrates in many subaqueous deltas are adapted to highly variable sediment deposition; therefore, rapid sedimentation is unlikely to disrupt this bioturbation. A more likely explanation for this change from stratified fabric (least recent) to bioturbated sediment (most recent) is a reduction of sediment supply, which would allow for bioturbation acting at the same rate to produce more pervasive mixing of sediments before bioturbated sediments are buried below the depth of bioturbation. This reasoning is also consistent with the observation of apparent downcore increases in SAR in cores PS17-84-MC and PS17-86-MC.

Downward increases in stratification and downcore reduction in apparent degree of bioturbation in both piston cores and multicores suggest that either the sediment supply to the region is declining, less deposited sediment is accumulating, the activities of bioturbating organisms are changing, or all the above. Although no time-series observations of bioturbation or benthic fauna are available, radioisotope geochronology combined with fabric analyses suggest that declining sediment supply and/or accumulation are a more robust explanation than changing bioturbation intensity. Results here suggest that the overall declining sediment accumulation began during the mid-20th century.

Geochronology analyses presented here for the area near the Virginia contrast with previous studies completed at sites within the MRDF region, using identical methods. In Duxbury et al., SARs were calculated at sites directly off Southwest Pass (water 30–80 m deep) and in deeper water (150–275 m) south of South Pass [28]. The ^{210}Pb SARs at Southwest Pass were 4.2–12.8 cm/y and at South Pass were 0.8–5.7 cm/y [28]. The ^{137}Cs values at Southwest Pass were 2.7–9.4 cm/y and at South Pass were 0.4–6.5 cm/y [28]. The study of Maloney et al. and references therein report similar SAR results, with cores taken ~7–12 km from Southwest Pass where ^{210}Pb SARs were 1.3–5.3 cm/y and with one station reaching 40.7 cm/y [2]. Values found by Duxbury et al. and references within Maloney et al. are substantially greater than those found around the Virginia, where ^{210}Pb SARs were 0.22–0.47 cm/y and 0.29–0.51 cm/y downcore. In the case of Duxbury et al., where values are ~90% higher than those found at the Virginia, core collection occurred over the same time frame, in similar seafloor morphology, and span both deeper and shallower water depths in locations off South Pass that fall at approximately the same distance from Southwest Pass [28]. A similar trend is present in ^{137}Cs accumulation rates, where the calculations of Duxbury et al. exceed those at the Virginia by ~90%, ~0.13 cm/y in this study compared with –1.59 cm/y found by Duxbury et al., [28].

4.3. Sediment Resuspension Potential from Combined Waves and Currents

Spatially, the greater MRDF shows declining sediment accumulation across multiple locations. Sediment resuspension and non-deposition of sediment in transport is one

possible explanation for the results above, if the present location of the Virginia lobe experiences higher bed-shear stresses than the locations of other nearby studies with higher SARs, and if the lobe has moved from a region of higher SARs to a region of lower SARs. This explanation would require that local wave-current bed-shear stresses are sufficient to resuspend deposited Mississippi river sediment plumes or prevent their initial deposition. Sha et al. have determined that shear stresses of 0.2–0.45 Pa are required to resuspend Mississippi river sediments that have been deposited (and experiencing consolidation) for 15–90 days, suggesting that lower shear stresses could prevent such sediments from depositing [29]. We are not aware of any benthic hydrodynamic or sediment transport studies conducted in the region, including studies cited in the extensive review of MRDF sedimentary processes by Maloney et al., so no direct measurements of local shear stresses appear to be available [2].

Results from the numerical modeling study by Zang et al. of sediment dynamics in the northern Gulf of Mexico from 1993 to 2012 include our study area and show that benthic hydrodynamic sedimentary processes on the MRDF are spatially and temporally heterogeneous, while also suggesting that the downslope motion of the Virginia lobe could possibly influence sediment deposition and thus SARs on the lobe [30]. Zang et al. found a zone on the MRDF of year-round elevated average bed-shear stresses of ~0.1 Pa from currents that are focused between and parallel to the 50 and 200 m isobaths [30].

Zang et al. also evaluated average seasonal sedimentation rates and lateral sediment fluxes through their models [30]. Near our study area, they found that fall and winter conditions are non-depositional despite elevated lateral sediment flux across the study area. In contrast, spring and summer conditions have high sediment flux, moderate sediment deposition (spring), and zero-to-low sediment deposition in summer. This combination of observations for sedimentation in our study area suggests that local heterogeneity of sediment supply and seabed hydrodynamics probably produces great heterogeneity in sediment bypass, resuspension, and accumulation, consistent with the hypothesis that downslope advection of the Virginia lobe (into a location of possibly stronger sediment resuspension/bypass), combined with historical decline in sediment supply, have altered the local depositional environment, yielding a decline in SARs over the last ~50 years. However, these collected results are not yet conclusive when evaluating this hypothesis due to uncertainties regarding Zang et al.'s model and the lack of direct observations. Future research and publications will likely include additional direct observations at this site and others across the MRDF, to further evaluate this hypothesis.

4.4. Estimating Total Gravity-Driven Mass Transport of the SS Virginia Sediment Lobe

Using mudflow dimensions estimated from bathymetric data (Figure 2), time-series estimates for the location of the Virginia shipwreck from Chaytor et al. and sediment properties from core data [6], it is possible to estimate lobe motion using a simplified block model and relevant sedimentary parameters, speed of motion for the lobe, total dry mass of sediment in that volume moving downslope, and rate of mass transport for different periods. Mudflows triggered by hurricane waves have been identified as the potential causes for the continuous movement of the Virginia from 2004 to 2008, occurring in short pulses of apparently rapid movement [6]. If these motions record the advection of the entire sediment lobe, as suggested by Chaytor et al., then a sediment volume likely greater than ~4 km^2 by >10 m thick (>40,000,000 m^3) is placed in motion by these events (approximate dimensions in Figure 2) [6]. For simplicity, Equation (5) assumes the mudflow lobe is rectangular, with dimensions of 2700 × 2700 m that were measured across bathymetric data (Figure 2). The volume and dry mass of the mudflow lobe were estimated using Equations (5) and (6):

$$v = L \cdot W \cdot z \quad (5)$$

$$\text{Dry mass} = v \cdot (1 - \varepsilon) \cdot 2.65 \quad (6)$$

where L is length, W is width, z is depth in meters, ε is porosity of bed, and 2.65 is the grain density in metric tons per m^3. Equation (7), from Whitehouse et al. was used to convert from bulk density to porosity [31]:

$$p_B = p + C_M ((p_s - p)/p_s) \quad (7)$$

where p_B is the bulk density, p is density of water (excluding sediment), p_s is the density of sediment grains, and C_M is the mass concentration (dry density) of sediment (mass/volume). Fractional porosity and bulk density were estimated from gamma density measurements for basal portions of sediment cores (Figure 8). The exact thickness for the action portion of the mudflow lobe is unknown; however, an approximate depth of ~16 m can be determined from the vertical difference from the toe of the youngest lobe to the average lobe surface in bathymetric data (Figure 2). Because we do not know if the entire lobe moves or just a portion, depth intervals of 100%, 50%, and 10% of 16 m will be used for the lobe height estimate. Under these conditions, the volume of the mudflow in motion is estimated to be 117×10^6, 58.3×10^6, and 11.6×10^6 m^3 for the 100%, 50%, 10% height estimates, respectively. From these values, Equation (7) was used to calculate the dry sediment mass of the mudflow lobe, yielding 124×10^6, 62×10^6, and 12×10^6 metric tons. When compared with the estimated annual sediment load of the Mississippi river, which is 210×10^6 metric tons per year, of which only 93.3×10^6 metric tons/y make it to Baton Rouge (upstream of diversions and outlets on the lower river [32], the dry mass values are approximately 120%, 66%, and 13% of the total yearly sediment load at Baton Rouge. Table 3 shows estimated total rates of sediment transport for the different active zone thicknesses to be 11–22,000 metric tons/y, depending on the slab thickness (estimated from the bathymetric dimensions shown in Figure 2), and that the speeds of motion are 182.5 m/y from 2004–2006, 18 m/y from 2006–2009, and 0.9 m/y from 2009–2016 (estimated from distances between locations of the Virginia over time as shown in Figure 8 of the study by Chaytor et al. [6]). Table 4 shows that the time required to displace 100% of the lobe volume at the three different speeds of lobe motion is ≥15 years. The time required to displace the volume equivalent for one year of sediment load at Baton Rouge (through a frontal area like that of the Virginia lobe) is ≥12 years. Finally, the time required to displace the volume equivalent for one year of sediment load at Baton Rouge across the entire MRDF, assuming that by enlarging the simple block model to an increased length allows us to consider transport rates across the entire MRDF region using a lobe width of 2.7 km and MRDF width of 100 km, is 0.03–0.12 years, at the rates of motion calculated from Figure 2.

Table 3. Mudflow lobe volume analysis and transport rates.

Depth Interval (m)	Lobe Volume Undergoing Transport ($\times 10^6$ m^3)	Dry Mass ($\times 10^6$ Metric Tons)	Percentage of Annual Sediment Load at Baton Rouge	Mass Transport Rate 2004–2006, Mt/y, Using Speed of 183 m/y (Figure 2), across Full Width of Lobe	Mass Transport Rate 2006–2009, Mt/y, Using Speed of 18 m/y (Figure 2), across Full Width of Lobe	Mass Transport Rate 2009–2016, Mt/y Using Speed of 0.9 m/y (Figure 2), across Full Width of lobe
16	120	120	120	22,000	2200	108
8	58	62	66	11,000	1100	56
1.6	12	12	13	2000	223	11

The amount of sediment exiting the main outlets of the Birdsfoot delta at Southwest and South Passes and Pass a Loutre is not currently well-defined. Based on Allison et al., the present sediment discharge is on the order of 45% of the suspended load presently passing New Orleans [15]. If the mass transport velocities for the Virginia lobe are extrapolated across the entire MRDF, then at least parts of the MRDF are being depleted of sediments by mudflow activity faster than they can be resupplied by sediments delivered from the main river outlets below the Head of Passes. Assuming sediment accumulation is a major

preconditioning or triggering factor, this suggests mudflow risk could decline in the future due to decreasing sediment accumulation on the MRDF and continued MRDF sediment depletion from mudflows.

Table 4. Mudflow lobe speed and transit time.

Speed of Flow (m/y)	Transit Time (y) to Evacuate Full Lobe Volume Past the Present Front of the Lobe	Transit Time (y) for a Volume Equivalent to One Year Sediment Load at Baton Rouge	Transit Time (y) for a Year-Equivalent Discharge Volume Across Entire Delta Front (If Front Is 100 km across, and Lobe Width Is 2 km)
183	15	12	0.06
18	149	120	0.60
0.9	2985	2407	12

Despite this, infrastructure on the seabed of the Gulf of Mexico is still in danger from mass movement events, especially infrastructure present in greater depths where flows that deplete sediment will continue to occur even if sediment accumulation continues to decline. The Virginia lobe currently lies 12 km upslope of eight pipelines [33]. On its current southwestern trajectory, the Virginia lobe will intersect a pipeline in ~5 km and seven more pipelines over ~12 km. Based on the transit time to evacuate the full lobe volume past the present front of the lobe (Table 4), the Virginia could overtake the pipelines in $\geq$28 years on its current trajectory. This would pose substantial environmental and economic risk if the pipelines and platforms are still in operation.

5. Conclusions

This study focuses on the WWII shipwreck SS Virginia and the underlying sediment lobe on the MRDF. Specifically, signs of recent deposition, mass failure, and overall migration of the shipwreck were examined. Analysis of sediment cores and geophysical data for the lobe beneath the shipwreck allowed a multifaceted approach by which to explore the sediment dynamics of the area. The major findings can be summarized as follows:

1. Sediment accumulation rates from ^{210}Pb and ^{137}Cs geochronology as well as relative indicators of sedimentation and bioturbation ascertained from core X-radiographs suggest that rates of sediment accumulation on the seabed surrounding the Virginia have declined since the mid-20th century.
2. Sediment accumulation rates are substantially lower than those of other nearby MRDF studies conducted using the same methods, such as that of Duxbury et al. and references within the study by Maloney et al., where rates are up to ~90% greater [2,28]. Using published models and data, a simple analysis of sediment resuspension potential from waves and currents suggests that annual-scale events can resuspend sediments, likely producing some combination of sediment resuspension, bypass, and possibly erosion that could help produce the low accumulation rates.
3. A volumetric analysis of the lobe combined with flow speeds calculated from the analysis undertaken by Chaytor et al. indicates that the Virginia lobe is moving at rates sufficient to evacuate the entire Virginia lobe volume over timescales of 7–1400 years [6]. If these rates are extrapolated across the entire MRDF and total mass transport is compared with fluvial sediment supply, results suggest that mudflows are moving sediment downslope at mass-transport rates far higher than the rate of annual sediment supply from the Mississippi river.

Author Contributions: Conceptualization, N.F. and S.J.B.; Methodology, N.F. and S.J.B.; Validation, N.F. and S.J.B.; Formal analysis, N.F. and S.J.B.; Data curation, N.F. and S.J.B.; Writing—original draft, N.F.; Writing—review & editing, N.F., S.J.B., J.D.C., K.X., N.J., I.Y.G., M.D., J.D., J.O. and J.M.; Visualization, N.F. and J.D.C.; Supervision, S.J.B.; Project administration, S.J.B.; Funding acquisition, S.J.B. and M.D. All authors have read and agreed to the published version of the manuscript.

Funding: This study was funded by the Department of the Interior, Bureau of Ocean Energy Management, under the cooperative agreements M13AC00013 and M22AC00015, with additional support from the Billy and Ann Harrison Endowment for Sedimentary Geology at Louisiana State University.

Data Availability Statement: Measurements made from collected cores during this study and analysis of data are available from the corresponding author upon reasonable request.

Acknowledgments: The authors would like to thank all those who provided guidance and resources throughout all stages of the project. Any use of trade, firm, or product names is for descriptive purposes only and does not imply endorsement by the U.S. Government.

Conflicts of Interest: The authors declare no conflict of interest.

References

1. Coleman, J.M.; Prior, D.B.; Louis, E.G. Submarine Landslides in The Mississippi River Delta. In Proceedings of the Offshore Technology Conference, Houston, TX, USA, 7–10 May 1978. [CrossRef]
2. Maloney, J.M.; Bentley, S.J.; Xu, K.; Obelcz, J.; Georgiou, I.Y.; Jafari, N.H.; Miner, M.D. Mass wasting on the Mississippi River Subaqueous Delta. *Earth-Sci. Rev.* **2020**, *200*, 103001. [CrossRef]
3. Maloney, J.M.; Bentley, S.J.; Xu, K.; Obelcz, J.; Georgiou, I.Y.; Miner, M.D. Mississippi River Subaqueous Delta is entering a stage of retrogradation. *Mar. Geol.* **2018**, *400*, 12–23. [CrossRef]
4. Gagliano, S.M.; Myer-Arendt, K.J.; Wicker, K.M. Land loss in the Mississippi River deltaic plain. *Gulf Coast Assoc. Geol. Soc. Trans.* **1981**, *31*, 295–300.
5. Kesel, R.H. Human modifications to the sediment regime of the Lower Mississippi River flood plain. *Geomorphology* **2003**, *56*, 3–4. [CrossRef]
6. Chaytor, J.; Baldwin, W.E.; Bentley, S.J.; Damour, M.; Jones, D.; Maloney, J.; Miner, M.; Obelcz, J.; Xu, K. *Short and Long-Term Movement of Mudflows of the Mississippi River Delta Front and Their Known and Potential Impacts on Oil and Gas Infrastructure*; Geological Society of London Special Publications: London, UK, 2020. [CrossRef]
7. Baldwin, W.E.; Ackerman, S.D.; Worley, C.R.; Danforth, W.W.; Chaytor, J.D. *High-Resolution Geo-Physical Data Collected along the Mississippi River Delta Front Offshore of Southeastern Louisiana*; US Geological Survey Field Activity 2017-003-FA; US Geological Survey: Reston, VA, USA, 2018. [CrossRef]
8. Baurick, T. 14-Year Taylor Energy Oil Leak Could Prove Larger than BP Spill, New Research Says. NOLA.com. 16 February 2019. Available online: https://www.nola.com/news/environment/14-year-taylor-energy-oil-leak-could-prove-larger-than-bp-spill-new-research-says/article_c160c6c8-fffd-5cc2-8a13-526978df20e8.html (accessed on 5 September 2022).
9. Guidroz, W.S. Subaqueous, Hurricane-Initiated Shelf Failure Morpho Dynamics along the Mississippi River Delta Front, North-Central Gulf of Mexico. Ph.D. Dissertation, Louisiana State University, Baton Rouge, LA, USA, 2009. Available online: https://digitalcommons.lsu.edu/gradschool_dissertations/1416 (accessed on 5 September 2022).
10. Nodine, M.C.; Gilbert, R.B.; Kiureghian, S.G.; Cheon, J.Y.; Wrzyszczynski, M.; Coyne, M.; Ward, E.G. Impact of Hurricane-Induced Mudslides on Pipelines. In Proceedings of the Offshore Technology Conference, Houston, TX, USA, 30 April–3 May 2007. [CrossRef]
11. Coleman, J.M.; Prior, D.B.; Garrison, L.E. *Subaqueous Sediment Instabilities in the Offshore Mississippi River Delta*; Bureau of Land Management, New Orleans OCS Office: Washington, DC, USA, 1980; p. 60.
12. Moore, D.G.; Scruton, P.C. Minor Internal Structures of Some Recent Unconsolidated Sediments. *AAPG Bull.* **1957**, *41*, 2723–2751.
13. Wright, L.D.; Nittrouer, C.A. Dispersal of river sediments in coastal seas: Six contrasting cases. *Estuaries* **1995**, *18*, 494. [CrossRef]
14. Walsh, J.P.; Corbett, D.R.; Mallinson, D.; Goni, M.; Dail, M.; Lowey, K.; Marcinak, K.; Ryan, K.; Smith, C.; Stevens, A.; et al. Mississippi Delta mudflow activity and 2005 Gulf Hurricanes. *Eos Trans. Am. Geophys. Union* **2006**, *87*, 477–478. [CrossRef]
15. Wright, L.D.; Friedrichs, C.T.; Kim, S.C.; Scully, M.E. Effects of ambient currents and waves on gravity-driven sediment transport on continental shelves. *Mar. Geol.* **2001**, *175*, 25–45. [CrossRef]
16. Allison, M.A.; Meselhe, E.A.; Kleiss, B.A.; Duffy, S.M. Impact of water loss on sustainability of the Mississippi River channel in its Deltaic Reach. *Hydrol. Process.* **2023**, *37*, e15004. [CrossRef]
17. Restreppo, G.A. Deltaic Wetland Dynamics from Seasonal to Centennial Scales. Ph.D. Dissertation, Louisiana State University, Baton Rouge, LA, USA, 2019. Available online: https://digitalcommons.lsu.edu/gradschool_dissertations/4828 (accessed on 23 August 2023).
18. Baker, S.R.; Friedman, G.M. A non-destructive core analysis technique using X-rays. *J. Sediment. Res.* **1969**, *39*, 1371–1383.
19. Corbett, D.R.; Mckee, B.; Duncan, D. An evaluation of mobile mud dynamics in the Mississippi River deltaic region. *Mar. Geol.* **2004**, *209*, 91–112. [CrossRef]
20. Cochran, J.K.; Masqué, P. Short-lived U/Th series radionuclides in the ocean: Tracers for scavenging rates, export fluxes and particle dynamics. In *Uranium-Series Geochemistry*; De Gruyter: Berlin, Germany, 2003; pp. 461–492. [CrossRef]
21. Nittrouer, C.A.; DeMaster, D.J.; McKee, B.A.; Cutshall, N.H.; Larsen, I.L. The effect of sediment mixing on Pb-210 accumulation rates for the Washington continental shelf. *Mar. Geol.* **1984**, *54*, 201–221. [CrossRef]
22. Berner, R.A. *Early Diagenesis: A Theoretical Approach*; Princeton University Press: Princeton, NJ, USA, 1980. [CrossRef]
23. Aller, R.C. Quantifying solute distributions in the bioturbated zone of marine sediments by defining an average microenvironment. *Geochim. Cosmochim. Acta* **1980**, *44*, 1955–1965. [CrossRef]

24. Nittrouer, C.A.; Sternberg, R.W. The formation of sedimentary strata in an allochthonous shelf environment: The Washington Continental Shelf. *Dev. Sedimentol.* **1981**, *32*, 201–232. [CrossRef]
25. Muhammad, Z.; Bentley, S.J.; Febo, L.A.; Droxler, A.W.; Dickens, G.R.; Peterson, L.C.; Opdyke, B.N. Excess 210Pb inventories and fluxes along the continental slope and basins of the Gulf of Papua. *J. Geophys. Res. Earth Surf.* **2008**, *113*, F01S17. [CrossRef]
26. Sommerfield, C.K.; Nittrouer, C.A.; Alexander, C.R. 7BE as a tracer of flood sedimentation on the Northern California Continental Margin. *Cont. Shelf Res.* **1999**, *19*, 335–361. [CrossRef]
27. Galloway, N.; Levy, T.; George, T. Mapping active mudflow features off Southwest Pass, Louisiana, Gulf of Mexico. In Proceedings of the Hydrographic Society of America 2017 Annual Meeting, Galveston, TX, USA, 20–23 March 2017; Available online: https://ushydro2019.thsoa.org/wp-content/uploads/2017/04/Galloway_Hydro2017_MappingMudflowFeatures-1.pdf (accessed on 2 September 2023).
28. Duxbury, J.; Bentley, S.J.; Xu, K. Temporal scales of mass wasting sedimentation across the Mississippi River Delta Front delineated by 210Pb/137Cs. *Geochronology*, 2023; *unpublished manuscript*.
29. Sha, X.; Xu, K.; Bentley, S.J.; Robichaux, P.A. Characterization and modeling of sediment settling, consolidation, and suspension to optimize coastal Louisiana Restoration. *Estuar. Coast. Shelf Sci.* **2018**, *203*, 137–147. [CrossRef]
30. Zang, Z.; Xue, G.; Kehui, X.; Bentley, S.J.; Chen, Q.; D'Sa, E.; Ge, Q. A Two Decadal (1993–2012) Numerical Assessment of Sediment Dynamics in the Northern Gulf of Mexico. *Water* **2019**, *11*, 938. [CrossRef]
31. Whitehouse, R.; Soulsby, R.; Roberts, W.; Mitchener, H. *Dynamics of Estuarine Muds: A Manual for Practical Applications*; Thomas Telford Publishing: Telford, UK, 2000.
32. Allison, M.A.; Demas, C.R.; Ebersole, B.A.; Kleiss, B.A.; Little, C.D.; Meselhe, E.A.; Powell, N.J.; Pratt, T.C.; Vosburg, B.M. A water and sediment budget for the lower Mississippi–Atchafalaya river in Flood Years 2008–2010: Implications for sediment discharge to the oceans and coastal restoration in Louisiana. *J. Hydrol.* **2012**, *432–433*, 84–97. [CrossRef]
33. Bureau of Ocean Energy Management. Pipelines. Geographic Mapping Data in Digital Format. 11 November 2023. Available online: https://www.data.boem.gov/Main/Mapping.aspx (accessed on 20 November 2023).